Escape of magma flow along the southern Central Asian Orogenic Belt prolonged lifetime of the Tarim mantle plume

Ke-Zhang Qin [1, 2*](秦克章), Ben-Xun Su [1, 2*](苏本勋), Franco Pirajno [3], Richard E. Ernst [4,5], Ya-Jing Mao [1](毛亚晶), Meng-Meng Cui [1, 2](崔梦萌), Jing Wang [1](王静), Fang-Lin Yuan [1](袁方林), Dong-Mei Tang [1](唐冬梅)

[1] Key Laboratory of Mineral Resources, Institute of Geology and Geophysics, Chinese Academy of Sciences, Beijing 100029, China

[2] University of Chinese Academy of Sciences, Beijing 100049, China

[3] Centre for Exploration Targeting, University of Western Australia, Crawley WA 6009, Australia

[4] Department of Earth Sciences, Carleton University Ottawa, ON, Canada K1S 5B6

[5] Novosibirsk State University, Novosibirsk 630090, Russia

Corresponding author: Ke-Zhang Qin，kzq@mail.iggcas.ac.cn

Escape of magma flow along the southern Central Asian Orogenic Belt prolonged lifetime of the Tarim mantle plume

Ke-Zhang Qin [1, 2*], Ben-Xun Su [1, 2*], Franco Pirajno [3], Richard E. Ernst [4,5], Ya-Jing Mao [1], Meng-Meng Cui [1, 2], Jing Wang [1], Fang-Lin Yuan [1], Dong-Mei Tang [1]

[1] Key Laboratory of Mineral Resources, Institute of Geology and Geophysics, Chinese Academy of Sciences, Beijing 100029, China

[2] University of Chinese Academy of Sciences, Beijing 100049, China

[3] Centre for Exploration Targeting, University of Western Australia, Crawley WA 6009, Australia

[4] Department of Earth Sciences, Carleton University Ottawa, ON, Canada K1S 5B6

[5] Novosibirsk State University, Novosibirsk 630090, Russia

Corresponding author: Ke-Zhang Qin，kzq@mail.iggcas.ac.cn; Ben-Xun Su, subenxun@mail.igcas.ac.cn

Abstract When a mantle plume is sited beneath a small craton and encountered ambient orogenic extension, what is likely to happen? Distinguished plume development and significant impact are revealed from geochronological and tectonic framework of the Tarim mantle plume and the mafic-ultramafic intrusions in southern Central Asian Orogenic Belt (CAOB). The mantle plume, which occurred beneath the Tarim Craton, one of the smaller cratons on Earth, lasted from 300 Ma to 270 Ma with peaks at 290 Ma and 278 Ma, which is unique compared to other plumes worldwide. Synchronously, the CAOB was at post-orogenic extension stage with an eastward propagating, scissor-like closure of the Paleo-Asian ocean. Numerous Ni-Cu sulfide deposits hosted in mafic-ultramafic intrusions, typically occurring in cratons and with a genetic affinity with plume events worldwide, are oddly concentrating along southern CAOB and have been termed as orogenic-type. These intrusions, associated with mafic dykes, show a decreasing trend in their numbers and a time lag (7-8 Ma) in formation age (295 to 255 Ma with peaks of 293 Ma, 282 Ma, and 271 Ma) with distance away from the Tarim Craton. Coincidentally, these orogenic gold deposits and intrusion associated mesothermal gold deposits also show a decreasing trens in their number and a time lag (10-20 Ma) in formation age (287 to 243 Ma with peaks of 277Ma, 254 Ma, and 268 Ma) with distance away from the Tarim Craton The unusual geochronological and tectonic links suggest that magmas of the Tarim mantle plume laterally escaped along extensional belts in southern CAOB, resulting in the formation of orogenic-style Ni-Cu sulfide deposits and with continuous magma supply to prolong the lifetime of the Tarim plume.

Keywords: Tarim mantle plume; magmatic Ni-Cu sulfide deposits; magma flow; post-orogenic extention; Central Asian Orogenic Belt

Most mantle plumes generally occur within large cratons and wide oceanic plates generating radial impacts on lithosphere mainly via plume heating, magma upwelling and subsequent eruptions (e.g., Hofmann and White, 1982; Ernst and Buchan, 2003). Mantle plumes have been suggested as the source of flood basalts (e.g., Campbell and Griffiths, 1990;

Hill et al., 1992; Lin and van Keken, 2005). These extremely rapid, large-scale eruptions of basaltic magmas have periodically formed continental flood basalt provinces on land and oceanic plateaus in ocean basins, together with coeval intrusive rocks being termed as large igneous provinces (LIPs) (Sheth, 1999; Campbell, 2005; Ernst et al., 2019). The formation of LIPs is often associated with continental rifting and breakup (Courtillot et al., 1999; Sengor and Natal'in, 2001; Ernst et al., 2005). This has led to the hypothesis that mantle plumes contribute to supercontinental breakup and the formation of ocean basins (Condie, 2001; Santosh et al., 2009; Pirajno and Santosh, 2014, 2015). Comprehensive empirical investigations and numerical modeling revealed that many mantle plumes, particularly Phanerozoic ones, took place over short time scales (less than 1 million years to several million years (e.g., Hill et al., 1992; Farnetani et al., 2018). In contrast, the Tarim plume differs from most plumes because of a long lifetime from 300 Ma to 270 Ma (e.g., Xu et al., 2013; Wei et al., 2014). It occurs within one of the smaller cratons on Earth (Fig. 1a) and has intensive interaction with the adjacent organic belts. The Tarim Craton was bounded by surrounding orogens in late Paleozoic when the mantle plume was active, and to its north the CAOB was being formed with an eastward propagating, scissor-like closure of the Paleo-Asian ocean and was plume-modified at contact with the Tarim Craton (Han and Zhao, 2018; Han et al., 2019). However it is difficult to identify mantle plume in orogenic belts (Puchkov et al.,2021). The magmatic records of the Tarim plume provide an ideal case to study the feature and influence of a mantle plume that impacted beneath a small craton and adjacent orogenic belts.

Accompanied by mantle plumes, various magmatic deposits associated with mafic-ultramafic rocks show a close spatial relationship with a coeval LIPs (Fig. 1a), and among these Ni-Cu sulfide deposits are the most common type. Most world-class magmatic Ni-Cu sulfide deposits are spatially within cratons and on their margins (Naldrett, 1999; Begg et al., 2010; Fig. 1a) and are temporally coeval with supercontinental breakup (Mail and Groves, 2011; Fig. 1b). Thus, they have been considered as a good indicator of mantle plume events. However, in last decades increasing numbers of Ni-Cu sulfide deposits discovered in orogenic settings, are primarily distributed in southern CAOB (Fig. 1a) and are unique in many aspects of tectonic settings compared to those in cratons and gave rise to debates on their genesis (Zhou et al., 2004; Han et al., 2010; Tang et al., 2011; Qin et al., 2013; Su et al., 2013; Sun et al., 2013; Wei et al., 2013; Mao et al., 2014; Xue et al., 2016a, 2016b; Cui et al., 2022). The orogenic-type Ni-Cu sulfide deposits and relevant mafic-ultramafic intrusions are interpreted to originate from melting of subduction-metasomatized mantle sources either due to post-orogenic extension and asthenopheric upwelling, followed by breakoff of earlier slab relicts (Song et al., 2011; Li et al., 2012), or due to the heating by the corresponding Tarim plume (Qin et al., 2011; Su et al., 2013; Mao et al., 2014). One of the unsolved issues is that such orogens with similar features to the CAOB were widely distributed on the earth throughout geological time, but rarely contain Ni-Cu sulfide deposits as those in southern CAOB. Geochronological and tectonic links between the Tarim plume and the deposit-hosting mafic-ultramafic intrusions deserve more attention to reveal the uniqueness of the Tarim plume and the orogenic-type Ni-Cu sulfide deposits.

The Ni-Cu sulfide deposits in the CAOB are mainly distributed in the southern margin, along the contacts with the Tarim Craton and North China Craton (Fig. 2a). In the CAOB there are numerous coeval non-mineralized mafic-ultramafic intrusions (Figs. 2b, c). The Eastern Tianshan-Beishan located to the northeast of the Tarim Craton hosts eleven economic Ni-Cu sulfide deposits and tens of barren intrusions (Fig. 2b). At least twelve Ni-Cu sulfide deposits have been explored in central Inner Mongolia, China (Fig. 2c; Ma et al., 2023), and several mafic-ultramafic intrusions are also exposed in the area between the Eastern Tianshan-Beishan and central Inner Mongolia, but these received very little investigations. In the eastermost of the CAOB, more than ten mafic-ultramafic intrusions are present surrounding the Hongqiling deposits (Wei et al., 2013; Cui et al., 2022). Along the Altai mountains, the mafic-ultramafic intrusions with Ni-Cu sulfide deposits are mainly found in Kalatongke, northwest China (Gao et al., 2012; Duan et al., 2007) and Maksut, eastern Kazakhstan (Khromykh et al., 2013) (Fig. 2a). All these mafic-ultramafic intrusions, except the Hongqiling ones, are Permian in age and have been genetically linked with the Tarim mantle plume based on their temporal coincidence and potential tectonic connection (e.g., Mao et al., 2006; Zhou et al., 2008; Polyakov et al., 2008; Pirajno, 2010, 2022; Qin et al., 2011; Su et al., 2011).

The Tarim LIP is mostly covered by the Gobi Desert and has an area of over 250,000 km^2 as revealed so far by drilling projects (Yang et al., 2005). It is dominated by a sequence of flood basalts (ca. 300 m thick on average) and also has kimberlites, Fe-Ti oxide ore-bearing layered mafic-ultramafic intrusions, bi-modal dyke swarms, alkaline igneous complexes (including syenites and A-type granites), pyroclastic rocks and rhyolites in the margins (Wei et al., 2014; Xu et al., 2014). Dating results indicate that the activity of the Tarim mantle plume commenced at 300 Ma and ended around 270 Ma with two phases of bimodal magmatism at 290 Ma and 278 Ma, respectively (Fig. 3; data source available in Supplementary materials). The kimberlites, as the first stage of magmatism, are the oldest unit with ages of 301-299 Ma (Zhang et al., 2013), while the mafic intrusive rocks (gabbro and diabase) and some rhyolites are the youngest with an age of ca. 270 Ma (Li et al., 2007; Tian et al., 2010). The ages of the basalts largely span from 297 Ma to 269 Ma (Zhang et al., 2010, 2012), and they, together with syenites and most rhyolites, are the main products of peak magmatisms (290 Ma and 278 Ma) of the Tarim mantle plume (Yang et al., 1996; Tian et al., 2010). These mafic rocks are high-Ti, alkali basaltic in composition, and some host low-grade V-Ti magnetite mineralization (Zhang and Zou, 2013; Wei et al., 2014).

The ages of the mafic-ultramafic intrusions in the Eastern Tianshan-Beishan vary from 290 Ma to 260 Ma with a peak at 282 Ma, and Ni-Cu sulfide mineralization occurred in a period of 284-282 Ma. The intrusions tend to locate in tectonically more active regions of the North Tianshan zone (Figs. 2b, 3; Qin et al., 2011; Su et al., 2011; Xue et al., 2016a). They have been explored as one of the most important Ni-Cu resource belts in China. In central Inner Mongolia, the intrusions are mainly distributed in the Baiyunebo rift and have formation ages of 285-258 Ma with a peak of 271 Ma, whilst the others are relatively older (294-291 Ma) (Figs. 2c, 3; Ma et al., 2023 and references therein). The Kalatongke Ni-Cu sulfide deposit has a formation age of 287 Ma (Han et al., 2004), and the intrusions in Maksut region formed mainly between 281 Ma and 278 Ma with one age of 293 Ma (Khromykh, 2007; Khromykh et al., 2013) (Fig. 3a). All the intrusions are low-Ti, tholeiitic basaltic in composition, explained as a counterpart of high-Ti, alkali basalts in the Tarim LIP (Qin et al., 2011), both of which are typical mantle plume magmatism occurs in the Emeishan LIP (Xu et al., 2014). These geochronologic results illustrate that the Permian mafic-ultramafic magmatism along the CAOB has a similar lifetime (30 Ma) and delays the Tarim mantle plume. Their age peaks (293 Ma, 282 Ma and 271 Ma) are respectively later, with a 7-8 Ma time lag, than a recommence age (300 Ma) and peak ages (290 Ma and 278 Ma) of the Tarim LIP (Fig. 3). The volumes, active ages and mineralization of these igneous activities display decreasing trends with distance away from the Tarim Craton (Figs. 2, 3), implying an outward weakening impact of the Tarim mantle plume.

Tectonically, the CAOB formed from an eastward propagating, scissor-like closure of the Paleo-Asian ocean, leading to collision between the Tarim and North China cratons in south and the Siberian Craton in north (Xiao et al., 2009, 2015; Eizenhöfer et al., 2014). In early Permian, orogeny had been almost completed in Western Tianshan and Altai as the west segments of the CAOB, and tectonic extention was restricted to regions between Precambrain microcontinents such as Kazakhstan, Yili and Kuluketage (Fig. 4a; Hu et al., 2000; Huang et al., 2015). Studies of early Permian A-type granitoids have well documented that the Tarim mantle plume merely affected the southwestern part of the assembled Tarim and Tianshan region (Han and Zhao, 2018; Han et al., 2019). were being rifted and well developing extentional and faulting tectonics, which subsequently occurred eastward along the southern CAOB (Xiao et al., 2015). Such tectonic framework provided favorable channels for magma movements. Widespread Permian mafic dykes in Bachu (Fig. 4b) and westernmost Beishan (Fig. 4c) probably represent accesses of magma surges from the Tarim mantle plume. In contrast, the Kunlun-Altyn orogens to the south of the Tarim Craton (Fig. 4a) are mature orogens and lack tectonic space, which would not be beneficial to magma intrusions (Fig. 4d).

The Permian mantle plume encountering the small Tarim Craton veered to flow beyond the cratonic margin into orogenic belts (Fig. 4d). The tectonics of the CAOB facilitated fast escape of magma and associated lateral expansion (Fig. 4e). Such magma movement would result in significant loss of both melt proportion and heat in the mantle plume head. This consequently leads to 1) a continuous supply of magma, which would prolong the lifetime of the plume, 2) low-degree partial melting of overlying the lithosphere and the plume head itself as well, producing high-Ti basalts (Fig. 4d). On the other hand, the parts of the CAOB where plume magma intruded were undergoing high-temperature heat flow. This, together with decompression related to post-orogenic extension, enhanced high-degree partial melting of the mantle source that had been metasomatized by subduction of the Paleo-Asian ocean (Su et al., 2011) (Fig. 4e).

According to this model, the variations of scale and number of mineral deposits between regions are likely correlated with magma volumes of the mantle plume and distance from the plume. The high-Mg tholeiitic melts close to the plume center (that is, the place with intensive contribution from the plume magma) would be much richer in compatible elements like Ni, which are favorable to forming deposits with high tenor of Ni sulfides. This may explain the relative high Fo olivine and high Ni sulfide in the Beishan and western Eastern Tianshan Ni-Cu deposits (e.g. Poyi, and Poshi, and Huangshannan deposits, Xue et al., 2016a; Mao et al., 2018) relative to those in the deposits in the eastern East Tianshan and Inner Mongolia (e.g., Tulaergen and Hulu deposits, Zhao et al., 2016; Mao et al., 2018; Ma et al., 2023). Regarding this aspect, the low Fo olivine (<80 mol%) and Ni sulfide tenor (<4 wt%) of the Permian mafic intrusions in the Kalatongke area, Altay region (Kang et al., 2020) might be explained by a far-end magmatism of the Tarim plume. However, this is not conclusive as there are few Permian magmatic records to trace the potential Tarim plume activity in the Altaids orgenic belt. We suggest that the Hongqiling deposits in the easternmost Central Asian Orogenic Belt (CAOB) are not the product of the Tarim mantle plume due to the much younger age (216 Ma) and farther distance to the Tarim Craton. If our model is applicable to the formation of many other orogenic-type Ni-Cu sulfide deposits worldwide, such as Vammala and Kotalahti in Finland (Barnes et al., 2009) and Aguablanca in Spain (Casquet et al., 2001) (Fig. 1a), the Hongqiling deposits might have a genetic affinity with the 250 Ma Siberian mantle plume considering distance and age issues, though more work is worth expanding further.

Mineral deposits along the CAOB mainly comprise both Ni-Cu and Au types. Notably, the porphyry and epithermal gold deposits primarily formed during the Devonian-Carboniferous accretion period, while most orogenic and intrusion-related mesothermal gold deposits emerged around the Carboniferous-Permian boundary or early Permian (Goldfarb et al., 2014; Qin et al., 2003, 1999). This transition marked the end of oceanic-arc subduction, initiating a phase characterized by large-scale strike-slip movement and a post-collision extensional environment, synchronized with the Tarim mantle plume activity (Qin et al., 2003, 2011;Su et al., 2011; Xu et al., 2001; Zhang et al., 2012).

Understanding fluid origins is crucial for analyzing gold deposit genesis. Orogenic gold deposits have two primary proposed origins. One is based on continental crust metamorphic fluid, relevant for Phanerozoic greenschist-facies terranes, while the other suggests a mantle fluid source, more disconnected from regional metamorphism and requiring deeper mantle sources for metal and heat supply (Wang et al., 2019). The proximity of most orogenic and intrusion-related mesothermal gold deposits to the Tarim Craton and their concurrent formation with the Tarim mantle plume hint at the plume's role in these deposits' formation.

The Western Tianshan region boasts several world-class Au deposits, with the Muruntau deposit in Uzbekistan being Asia's largest. Various isochron ages for Muruntau and other deposits like Zarmitan and Katbasu have been reported, ranging from around 322.5 Ma to 240 Ma. In contrast, the Eastern Tianshan region hosts deposits like Kanggur, Hongshi, and Hongshan, with mineralization ages predominantly between 290 Ma and 246.5 Ma. Beishan ore belt features the Yueyashan and Laodonggou gold-polymetallic deposits, with ages primarily in the 243 Ma to 233.8 Ma range. In west Inner Mongolia, the Xiaerchulu, Zhulazhaga, and Changshanhao deposits are Permian magmatic hydrothermal gold types, with dating results spanning from 291.48 Ma to 246 Ma.

Considering the Tarim mantle plume's activity from 300 Ma to 270 Ma, it appears the formation of CAOB gold deposits was influenced by this tectonic-magmatic activity. This influence seems to have propagated from west to east and weakened over distance. Geographically, the CAOB in China spans from the Tianshan areas, through the Junggar basin, to the Altay terranes. The Tianshan area further divides into South, Central, and North Tianshan mountains. West Junggar houses significant epithermal gold deposits like the Baogutu porphyry and Hatu epithermal deposits, with mineralization ages varying from around 341.6 Ma to 290 Ma. The Altay orogenic belt, which encompasses the Altay terrain and Erqis accretionary complex, features orogenic gold deposits like Duolanasayi and Saidu, formed mainly during the Late Carboniferous-Early Permian.

Statistically, the gold deposits in South Tianshan mountains, primarily of the orogenic type like Muruntau and Zarmitan, formed around 290-275 Ma. In contrast, the North Tianshan mountains, which include deposits like Wangfeng, Saridala, and Katbasu, mainly formed around 270-255 Ma. The Central Tianshan mountains' gold deposits formed in two major phases, around 290-285 Ma and 265-255 Ma.

Acknowledgments This study was financially supported by the Strategic Priority Reseach Program of the Chinese Academy of Aciences (XDA0430302), the National Key R&D Program of China (2022YFC2903501), the Nature Science Foundation of China (41830430), and the Youth Innovation Promotion Association, Chinese Academy of Sciences.

References (more references relevant to age data available in Supplementary materials)

Barnes, S.J., Makkonen, H.V., Dowling, S.E., Hill, R.E., Peltonen, P., 2009. The 1.88 Ga Kotalahti and Vammala nickel belts, Finland: geochemistry of the mafic and ultramafic metavolcanic rocks. Bulletin of the Geological Society of Finland 81, 103-141.

Campbell, I.H., Griffiths, R.W., 1990. Implications of mantle plume structure for the evolution of flood basalts. Earth Planetary Science Letters 99, 79-93.

Campbell, I.H., 2005. Large igneous provinces and the mantle plume hypothesis. Elements 1, 265-269.

Casquet, C., Galindo, C., Tornos, F., Velasco, F., Canales, A., 2001. The Aguablanca Cu-Ni ore deposit (Extremadura, Spain), a case of synorogenic orthomagmatic mineralization: age and isotope composition of magmas (Sr, Nd) and ore (S). Ore Geology Reviews 18, 237-250.

Condie, K.C., 2001. Mantle plumes and their record in Earth history. Cambridge University Press.

Cui, M.M., Su, B.X., Wang, J., Tang, D.M., Sakyi, P.A., Moynier, F., 2022. Linking selective alteration, mineral compositional zonation and sulfide melt emplacement in orogenic-type magmatic Ni-Cu sulfide deposits. Journal of Petrology 63, egac043.

Ernst, R.E., Buchan, K.L., 2003. Recognizing mantle plumes in the geological record. Annual Review of Earth and Planetary Sciences 31, 469-523.

Ernst, R.E., Buchan, K.L., Campbell, I.H., 2005. Frontiers in large igneous province research. Lithos 79, 271-297.

Ernst, R.E., Liikane, D.A., Jowitt, S.M., Buchan, K., Blanchard, J., 2019. A new plumbing system framework for mantle plume-related continental Large Igneous Provinces and their mafic-ultramafic intrusions. Journal of Volcanology Geothermal Research 384, 75-84.

Fang, S., Wu, Z., Yu, H., 2017. Tectonic map of Inner Mongolia (1:1500000). Wuhan: China University of Geosciences Press (in Chinese).

Farnetani, C.G., Hofmann, A.W., Duvernay, T., Limare, A., 2018. Dynamics of rheological heterogeneities in mantle plumes. Earth Planetary Science Letters 499, 74-82.

Gao, J.F., Zhou, M.F., Lightfoot, P.C., Wang, C.Y., Qi, L., 2012. Origin of PGE-poor and Cu-rich magmatic sulfides from the Kalatongke deposit, Xinjiang, northwest China. Economic Geology 107, 481-506.

Han, Y., Zhao, G., 2018. Final amalgamation of the Tianshan and Junggar orogenic collage in the southwestern Central Asian Orogenic Belt: Constraints on the closure of the Paleo-Asian Ocean. Earth-Science Reviews 186, 129-152.

Han, Y., Zhao, G., Cawood, P.A., Sun, M., Liu, Q., Yao, J., 2019. Plume-modified collision orogeny: The Tarim-western Tianshan example in Central Asia. Geology 47, 1001-1005.

Hill, R., Campbell, I., Davies, G., Griffiths, R., 1992. Mantle plumes and continental tectonics. Science 256, 186-193.

Hofmann, A.W., White, W.M., 1982. Mantle plumes from ancient oceanic crust. Earth Planetary Science Letters 57, 421-436.

Hu, A.Q., Jahn, B.M., Zhang, G.X., Chen, Y.B., Zhang, Q.F., 2000. Crustal evolution and Phanerozoic crustal growth in northern Xinjiang: Nd isotopic evidence. Part I. Isotopic characterization of basement rocks. Tectonophysics 328, 15-51.

Huang, Z.Y., Long, X.P., Kröner, A., Yuan, C., Wang, Y.J., Chen, B., Zhang, Y.Y., 2015. Neoproterozoic granitic gneisses in the Chinese Central Tianshan Block: Implications for tectonic affinity and Precambrian crustal evolution. Precambrian Research 269, 73-89.

Kang, Z., Qin, K.Z., Mao, Y.J., Tang, D.M., Yao, Z.S., 2020. The formation of a magmatic Cu-Ni sulfide deposit in mafic intrusions at the Kalatongke, NW China: Insights from amphibole mineralogy and composition. Lithos 352-353, 105317.

Li, C.S., Zhang, M.J., Fu, P., Qian, Z.Z., Hu, P.Q., Ripley, E.M., 2012. The Kalatongke magmatic Ni-Cu deposits in the Central Asian Orogenic Belt, NW China: product of slab window magmatism? Mineralium Deposita 47, 51-67.

Lin, S.C., van Keken, P.E., 2005. Multiple volcanic episodes of flood basalts caused by thermochemical mantle plumes. Nature 436, 250-252.

Maier, W.D., Groves, D.I., 2011. Temporal and spatial controls on the formation of magmatic PGE and Ni-Cu deposits. Mineralium Deposita 46, 841-857.

Pirajno, F., Santosh, M., 2015. Mantle plumes, supercontinents, intracontinental rifting and mineral systems. Precambrian Research 259, 243-261.

Pirajno, F., 2010. Intracontinental strike-slip faults, associated magmatism, mineral systems and mantle dynamics: examples from NW China and Altay-Sayan (Siberia). Journal of Geodynamics 50, 325-346.

Pirajno, F., 2022. Mineral systems and their putative link with mantle plumes. Geological Society, London, Special Publications 518, 467-492.

Puchkov, V.N., Ernst, R.E., Ivanov, K.S. (2021) The importance and difficulties of identifying mantle plumes in orogenic belts: An example based on the fragmented large igneous province (LIP) record in the Ural fold belt. Precambrian Research, v. 361, 106186.

Qin, K.Z., Su, B.X., Sakyi, P.A., Tang, D.M., Li, X.H., Sun, H., Xiao, Q.H., Liu, P.P., 2011. SIMS Zircon U-Pb geochronology and Sr-Nd isotopes of Ni-Cu bearing mafic-ultramafic intrusions in Eastern Tianshan and Beishan in correlation with flood basalts in Tarim Basin (NW China): constraints on a ca. 280 Ma mantle plume. American Journal of Science 311, 237-260.

Santosh, M., Maruyama, S., Yamamoto, S., 2009. The making and breaking of supercontinents: some speculations based on superplumes, super downwelling and the role of tectosphere. Gondwana Research 15, 324-341.

Sengor, A.M.C., Natal'in, B.A., 2001. Rifts of the world. In: Ernst, R.E., Buchan, K.L. (Eds.), Mantle Plumes: Their Identification Through Time, Special Paper, vol. 352. Geological Society of America, Boulder, 389-482.

Sheth, H., 1999. Flood basalts and large igneous provinces from deep mantle plumes: fact, fiction, and fallacy. Tectonophysics 311, 1-29.

Su, B.X., Qin, K.Z., Tang, D.M., Sakyi, P.A., Liu, P.P., Sun, H., Xiao, Q.H., 2013. Late Paleozoic mafic-ultramafic intrusions in southern Central Asian Orogenic Belt (NW China): insight into magmatic Ni-Cu sulfide mineralization in orogenic setting. Ore Geology Reviews 51, 57-73.

Wei, B., Wang, C.Y., Li, C.S., Sun, Y.L., 2013. Origin of PGE-depleted Ni-Cu sulfide mineralization in the Triassic Hongqiling No. 7 orthopyroxenite intrusion, Central Asian Orogenic Belt, northeastern China. Economic Geology 108, 1813-1831.

Xiao, W., Windley, B., Yuan, C., Sun, M., Han, C., Lin, S., Chen, H., Yan, Q., Liu, D., Qin, K., 2009. Paleozoic multiple subduction-accretion processes of the southern Altaids. American Journal of Science 309, 221-270.

Xiao, W.J., Windley, B.F., Sun, S., Li, J.L., Huang, B.C., Han, C.M., Yuan, C., Sun, M., Chen, H., 2015. A tale of amalgamation of three Permo-Triassic collage systems in Central Asia: Oroclines, sutures, and terminal accretion. Annual Review of Earth Planetary Sciences 43, 477-507.

Xu, Y.G., Wei, X., Luo, Z.Y., Liu, H.Q., Cao, J., 2014. The Early Permian Tarim Large Igneous Province: main characteristics and a plume incubation model. Lithos 204, 20-35.

Zhang, C.L., Zou, H.B., 2013. Comparison between the Permian mafic dykes in Tarim and the western part of Central Asian Orogenic Belt (CAOB), NW China: Implications for two mantle domains of the Permian Tarim Large Igneous Province. Lithos 174, 15-27.

Cao, Y., Nie, F., Xiao, W., Liu, Y., Zhang, W., Wang, F., 2014. Metallogenic age of the Changshanhao gold deposit in Inner Mongolia，China. Acta Petrol. Sin. 30, 2092–2100.

Chen, W., Zhang, Y., Qin, K., Wang, Q., Wang, Y., Liu, X., 2007. Study on the age of the shear zone-type gold deposit of East Tianshan, Xinjiang, China. Acta Petrol. Sin. 23, 2007–2016.

Chen, Y.-J., Chen, H.-Y., Zaw, K., Pirajno, F., Zhang, Z.-J., 2007. Geodynamic settings and tectonic model of skarn gold deposits in China: An overview. Ore Geol. Rev. 31, 139–169. https://doi.org/10.1016/j.oregeorev.2005.01.001

Cheng, Z., Rui, X., 1996. Minerogenetic characteristics of Saidu gold deposit in Habahe country. Xinjiang Geol. 14, 247–254.

Cui, H., Chen, Z., 1996. Geology of gold deposits in Beishan,Gansu. Geological Publishing House, Beijing.

Deng, J., Wang, Q., 2016. Gold mineralization in China: Metallogenic provinces, deposit types and tectonic framework. Gondwana Res. 36, 219–274. https://doi.org/10.1016/j.gr.2015.10.003

Dong, L., Wan, B., Yang, W., Deng, C., Chen, Z., Yang, L., Cai, K., Xiao, W., 2018. Rb-Sr geochronology of single gold-bearing pyrite grains from the Katbasu gold deposit in the South Tianshan, China and its geological significance. Ore Geol. Rev. 100, 99–110. https://doi.org/10.1016/j.oregeorev.2016.10.030

Gao, Y., Zhang, Z., Wang, Z., Yang, W., Ban, J., Dong, F., Tan, W., 2015. Geochronology of the Katabaasu gold deposit in West Tian Shan and its geological significance: Evidence from 40Ar － 39Ar isotopic ages of sericit. Geol. Explor. 51, 0805–0815.

Goldfarb, R.J., Taylor, R.D., Collins, G.S., Goryachev, N.A., Orlandini, O.F., 2014. Phanerozoic continental growth and gold metallogeny of Asia. Gondwana Res. 25, 48–

102. https://doi.org/10.1016/j.gr.2013.03.002
Kempe, U., Belyatsky, B., Krymsky, R., Kremenetsky, A., Ivanov, P., 2001. Sm–Nd and Sr isotope systematics of scheelite from the giant Au(–W) deposit Muruntau (Uzbekistan): implications for the age and sources of Au mineralization. Miner. Deposita 36, 379–392. https://doi.org/10.1007/s001260100156
Li, H., Chen, F., 2004a. Regional Mineralization in Altay Area of Northern Xinjiang China. Geological Publishing House, Beijing.
Li, H., Chen, F., 2004b. Isotopic, geochronology of regional mineralization in Xinjiang,China. Geological Publishing House, Beijing.
Li, H., Chen, F., Jiang, H., 2000. Study on Rb-Sr Isotopic Ages of Gold Deposits in West Junggar Area, Xinjiang. Acta Geol. Sin. 74, 181–192.
Li, H., Xie, C., Chang, H., 1998a. Mineralization in Altay Area of Nonferrous and Noble Metal of Northern Xinjiang China. Geological Publishing House, Beijing.
Li, H., Xie, C., Chang, H., 1998b. Study on metallogenetic chronology of nonferrous and precious meltallic ore deposits in North Xinjiang,China. Geological Publishing House, Beijing.
Li, J., 2006. Regional Metallogenic System of Alashan Block in Inner Monolia Autonomous Region (PhD). China University of Geoscience(Beijing).
Li, J., Luo, H., Zhou, H., Sang, H., Qin, Z., Wang, S., Sun, Z., 2004. Metallogenic epoch of Zhulazaga gold deposit in Alxa area,Inner Mongolia Autonomous Region. Geochimica 33, 663–669.
Lu, Y., Zhang, Y., Pan, M., Fan, J., Liu, Y., Zhang, D., Chen, X., Pan, A., 2010. Types and

geological characteristics of gold deposits in East Junggar,Xinjiang. Acta Geosci. Sin. 31, 434–442.

Mao, J., Konopelko, D., Seltmann, R., Lehmann, B., Chen, W., Wang, Y., Eklund, O., Usubaliev, T., 2004. Postcollisional Age of the Kumtor Gold Deposit and Timing of Hercynian Events in the Tien Shan, Kyrgyzstan. Econ. Geol. 99, 1771–1780. https://doi.org/10.2113/gsecongeo.99.8.1771

Morelli, R., Creaser, R.A., Seltmann, R., Stuart, F.M., Selby, D., Graupner, T., 2007. Age and source constraints for the giant Muruntau gold deposit, Uzbekistan, from coupled Re-Os-He isotopes in arsenopyrite. Geology 35, 795. https://doi.org/10.1130/G23521A.1

Nie, F., Jiang, S., Liu, Y., Zhang, Y., Zhao, Y., 2003. Ore-fluid evolution of the Xiaoxigong gold deposit hosted in Proterozoic metamorphic rocks,Gansu Province,as deduced from sulfur oxygen hydrogen and lead isotopic evidence. Geol. Geochem. 31, 1–10.

Qin, K Z., Xiao, W J., Xu, X W., Yan, Z., Mao, J W., 2003. Overview of major Au, Cu, Ni and Fe deposits and metallogenic evolution of the eastern Tianshan Mountains, Northwestern China.pdf, in: IAGOD Guidebook Series 10. Presented at the Tectonic Evolution and Metallogeny of the Chinese Altay and Tianshan Proceedings Volume of the International Symposium of the IGCP-473 Project in Urumqi and Guidebook of the Field Excursion in Xinjiang,China, Cercams, London, pp. 227–148.

Qin, K Z., Sun, S., Chen, H., Hao, J., 1999. Temporal-spatial distribution framework of metal deposits in northern Xinjiang: As guides of Paleozoic archipelago-type collision orogenic belts. In: Chen H.H. et al ed. Collision Orogenic Belts of China. Beijing. Collis. Orog. Belts China 183–196.

Seltmann, R., Konopelko, D., Biske, G., Divaev, F., Sergeev, S., 2011. Hercynian post-collisional magmatism in the context of Paleozoic magmatic evolution of the Tien Shan orogenic belt. J. Asian Earth Sci. 42, 821–838. https://doi.org/10.1016/j.jseaes.2010.08.016

Shen, Y.C., Jin, C.W., 1993. Magmatism and Gold Mineralization in Western Junggar. Beijing Science Press, pp. 113–172 (in Chinese with English abstract)

Shen, P., Shen, C., Pan, C., Pan, H., Dai, H., Meng, 2010. Zircon age and metallogenic characteristics of the Hatu-Baogutu Au-Cu metallogenic concentric region in Xinjiang. Acta Petrol. Sin. 26, 2875–2893.

Shen, P., Shen, Y., Li, X.-H., Pan, H., Zhu, H., Meng, L., Dai, H., 2012. Northwestern Junggar Basin, Xiemisitai Mountains, China: A geochemical and geochronological approach. Lithos 140–141, 103–118. https://doi.org/10.1016/j.lithos.2012.02.004

Shen, Y., Jin, C., 1993. Magmatism and gold Mineralization in Western Junggar. Science Press, Beijing.

Shu, L., Charvet, J., Ma, R., 1998. Study of a large scall Paleozoic dextral strike-slip ductile shear zone along the northern margin of the central Tianshan，Xinjiang. Xinjiang Geol. 16, 326–336.

Wang, J., Liu, J., Jiang, X., Wang, B., Jiang, S., 2011. Ar40-Ar39 age and its significance of haoxiaoerhutong gold deposit in Inner Mongolia. Acta Mineral. Sin. 31, 643–644.

Wang, J., Nie, F., Zhang, X., Liu, Y., Liu, C., Ding, C., 2014. Re-Os isotopic dating of molybdenite separated from the Xiaerchulu Au deposit,Inner Mongolia and the mineralization. Acta Geolocical Sin. 88, 2386–2393.

Wang, J., Nie, F.-J., Zhang, X., Jiang, S., 2016. Molybdenite Re–Os, zircon U–Pb dating and Lu–Hf isotopic analysis of the Xiaerchulu Au deposit, Inner Mongolia Province, China. Lithos 261, 356–372. https://doi.org/10.1016/j.lithos.2016.06.008

Wang, Q., Deng, J., Zhao, H., Yang, L., Ma, Q., Li, H., 2019. Review on orogenic gold deposits. Earth Sci. 44, 2155–2186.

Wilde, A.R., Layer, P., Mernagh, T., Foster, J., 2001. The Giant Muruntau Gold Deposit: Geologic, Geochronologic, and Fluid Inclusion Constraints on Ore Genesis. Econ. Geol. 96, 633–644. https://doi.org/10.2113/gsecongeo.96.3.633

Xiao, W., Nie, F., Liu, Y., 2012. Isotope geochronology study of the granitoid intrusions in the Changshanhao gold deposit and its geological implications. ACTA Petrol. Sin. 28, 535–543.

Xu, B., Lu, Y., Gu, X., Zhang, W., 2009. Metallogenic epoc of the Shuangquan gold deposit in Qitai area, Xinjiang, china. Geol. Bull. China 28, 1871–1884.

Xu, Y., Chung, S.-L., Jahn, B., Wu, G., 2001. Petrologic and geochemical constraints on the petrogenesis of Permian–Triassic Emeishan flood basalts in southwestern China. Lithos 58, 145–168. https://doi.org/10.1016/S0024-4937(01)00055-X

Yan, S., Chen, W., Wang, Y., Zhang, Z., Chen, B., 2004. 40Ar/39Ar Dating and Its Significance of the Ertix Gold Metallogenic Belt in the Altay Orogen, Xinjiang. Acta Geol. Sin. 78, 500–506.

Yuan, F., Deng, Y.-F., Zhou, T., Zhang, D., Xu, C., Jowitt, S.M., Zhang, R., Zhao, B., 2017. Petrogenesis and timing of emplacement of porphyritic monzonite, dolerite, and basalt associated with the Kuoerzhenkuola Au deposit, Western Junggar, NW China:

implications for early Carboniferous tectonic setting and Cu-Au mineralization prospectivity. Int. Geol. Rev. 59, 1154–1174. https://doi.org/10.1080/00206814.2016.1263976

Zhang, D., Zhou, T., Yuan, F., Jowitt, S.M., Fan, Y., Liu, S., 2012. Source, evolution and emplacement of Permian Tarim Basalts: Evidence from U–Pb dating, Sr–Nd–Pb–Hf isotope systematics and whole rock geochemistry of basalts from the Keping area, Xinjiang Uygur Autonomous region, northwest China. J. Asian Earth Sci. 49, 175–190. https://doi.org/10.1016/j.jseaes.2011.10.018

Zhang, G., Zhang, Y., Xin, H., Huang, C., Niu, W., Duan, L., Zhao, Z., Ren, B., 2021. Geochronology and geochemistry of diorite porphyrite from Laodonggou gold-polymetallic deposit, Beishan, Inner Mongolia, and its metallogenic significance. Miner. Depos. 40, 555–573.

Zhang, L., Liu, T., Shen, Y., Li, G., Ji, J., 2002. Isotopic Geochronology of the Late Paleozoic Kanggur Gold Deposit of East Tianshan Mountains, Xinjiang, NW China. Resour. Geol. 52, 249–261. https://doi.org/10.1111/j.1751-3928.2002.tb00135.x

Zhang, L.-C., Xiao, W.-J., Qin, K.-Z., Ji, J., Yang, X., 2004. Types, geological features and geodynamic significances of gold-copper deposits in the Kanggurtag metallogenic belt, eastern Tianshan, NW China. Int. J. Earth Sci. 93, 224–240. https://doi.org/10.1007/s00531-004-0383-x

Zhang, Q., Xue, C., Feng, B., Xing, H., Mo, X., Zhao, S., Yang, W., Xing, L., 2015. Geology, geochemistry and metallogenic epoch of the Katebasu large-sized gold deposit, Western Tianshan Mountains, Xinjiang. Geol. China 42, 411–437.

Figure captions

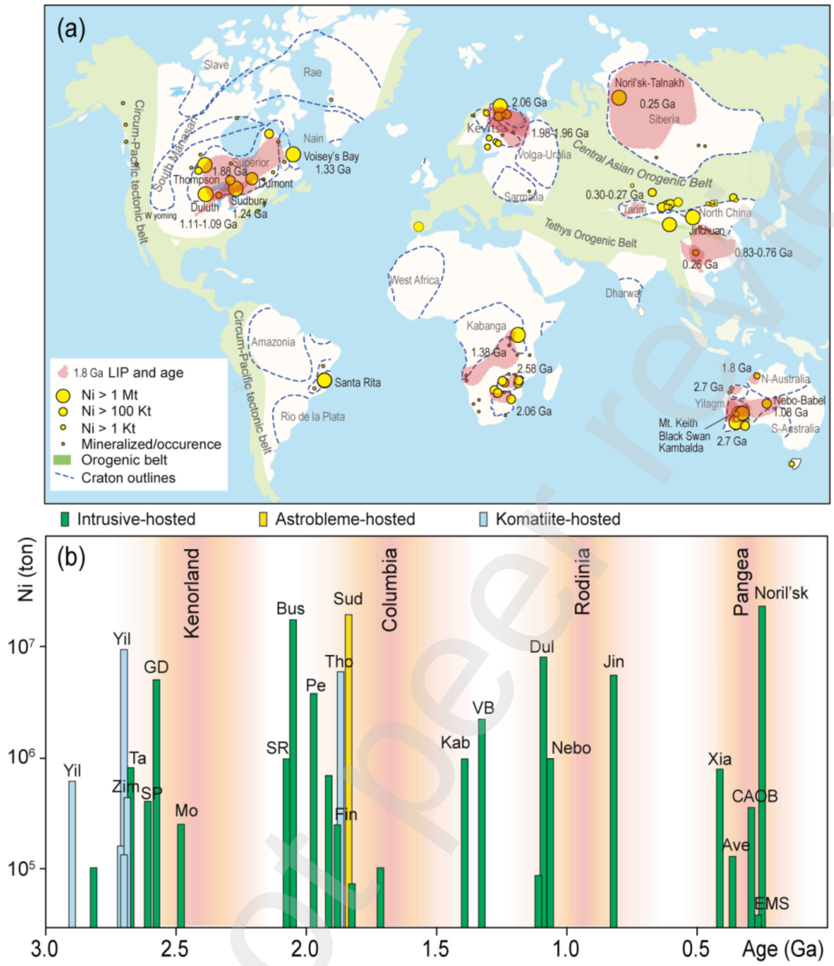

Fig. 1 (a) Distribution of Ni-Cu sulfide deposits (in yellow) worldwide (modified after Maier and Groves, 2011) and correspondingly coeval large igneous provinces (LIPs; in brown) with ages (modified after Ernst and Youbi, 2017). (b) Secular distribution of Ni-Cu sulfide deposits and their correlation with periods of super-continent amalgamation and break-up (modified after Maier and Groves, 2011 and references therein). Ave, Avebury; Bus, Bushveld; Dul, Duluth; Fin, Finnish Ni belt; GD, Great Dyke; Jin, Jinchuan; Kab, Kabanga; Mo, Monchegorsk; Nebo, Nebo-Babel; Pe, Pechenga; SP, Selebi Phikwe; SR, Santa Rita; Sud, Sudbury; Ta, Tati; Tho, Thompson; VB, Voisey's Bay; Yil, Yilgarn; Zim, Zimbabwe; Xia,

Xiarihamu; CAOB, Central Asian Orogenic Belt; EMS, Emeishan.

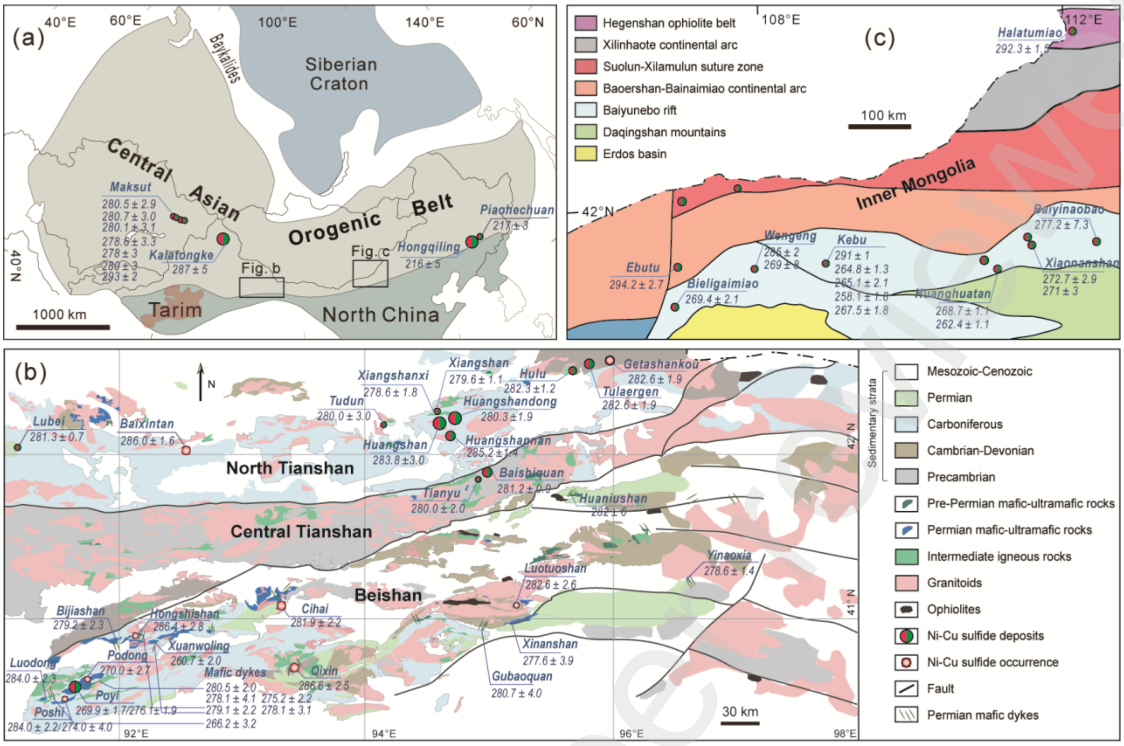

Fig. 2 (a) Simplified map showing Central Asian Orogenic Belt and its sourrounding cratons (modified after Xiao et al., 2009). Distribution of mafic-ultramafic intrusions with ages in (b) Eatern Tianshan (including North and Central Tianshan) and Beishan (modified after Xue et al., 2016a), and in (c) central Inner Mongolia (modified after Fang et al., 2017). Age data (Ma) are available in Supplementary materials.

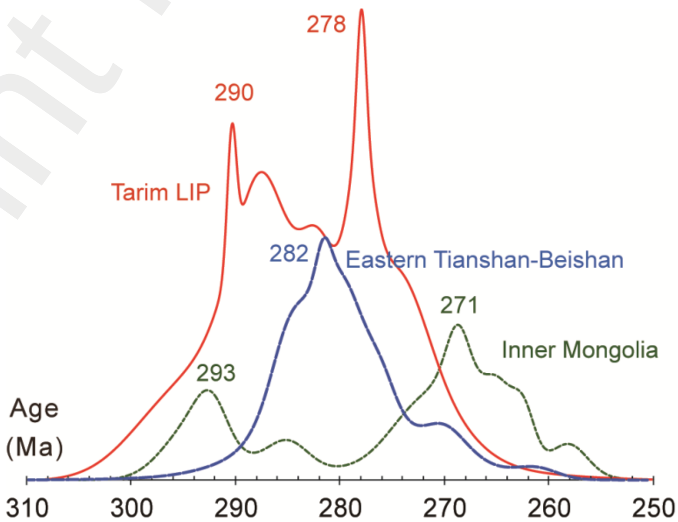

Fig. 3 Histogram of ages of mafic-ultramafic rocks from the Tarim LIP, Eastern Tianshan-

Beishan and central Inner Mongolia.

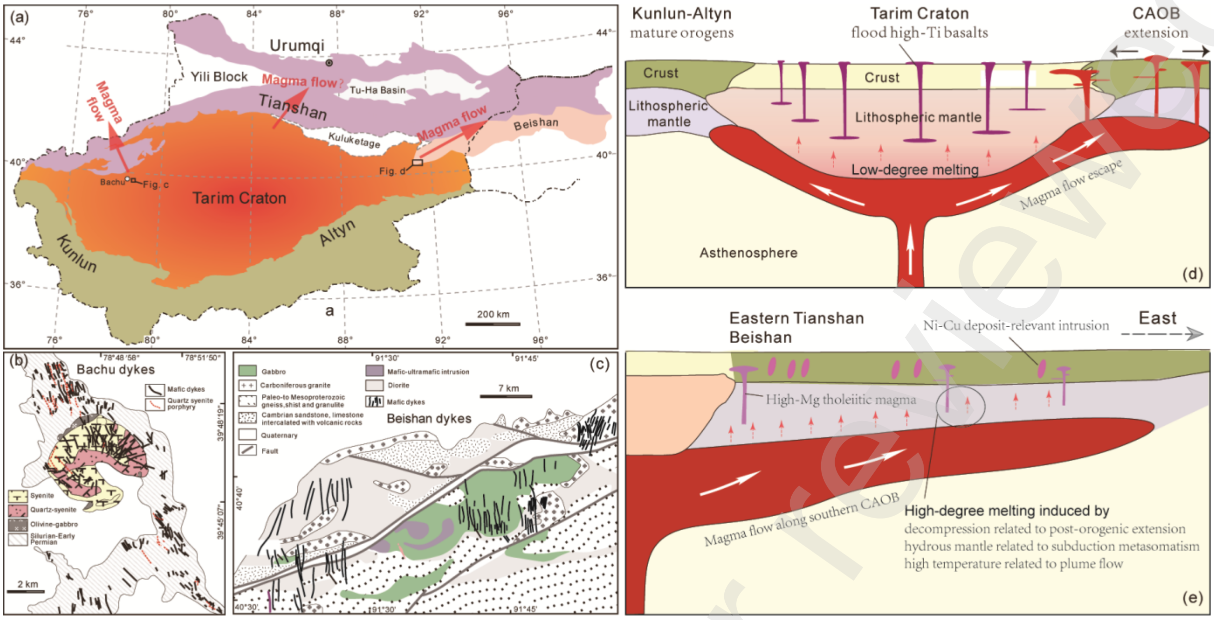

Fig. 4 (a) Tectonic framework of the Tarim Craton (modified after Wei et al., 2014), and distribution of mafic dykes in (b) Bachu (after Wei et al., 2014) and (c) westernmost Beishan (after Xue et al., 2016b). (d, e) Models of the Tarim mantle plume and escape of magma flows along the CAOB.

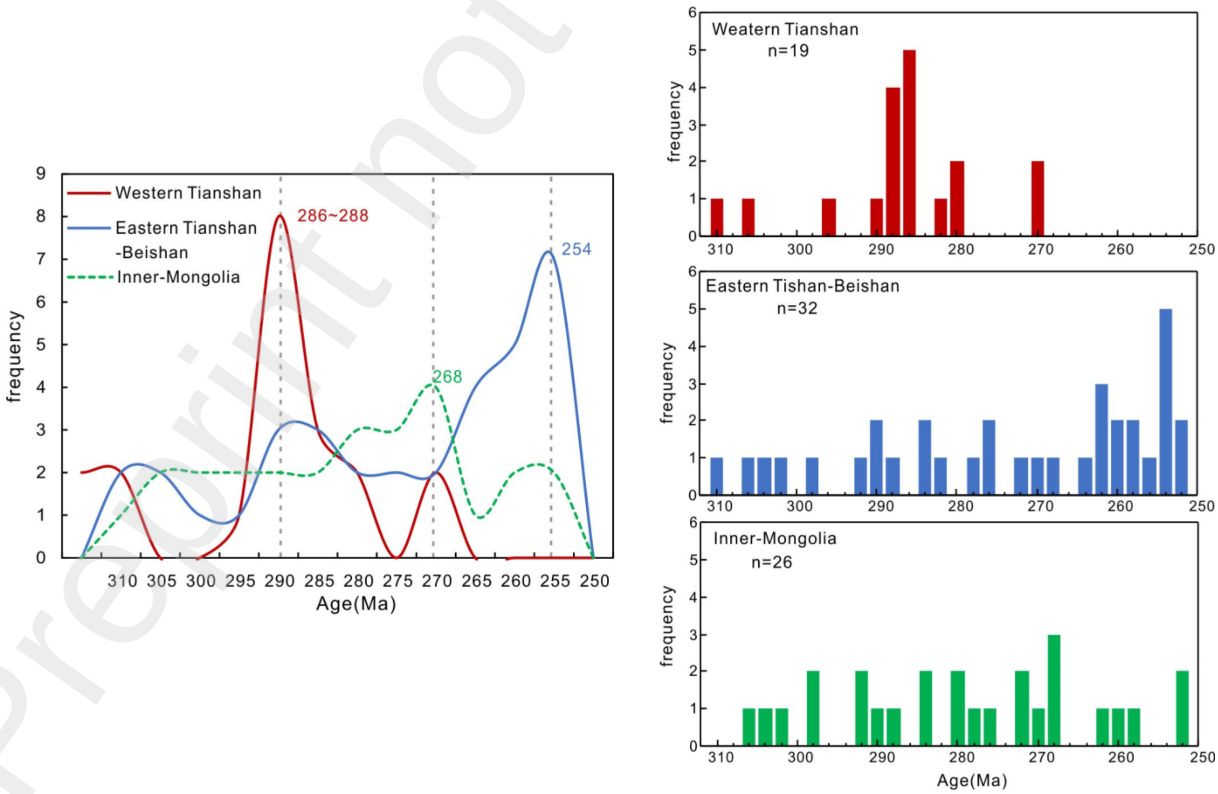

Fig. 5 Histogram of ages of gold deposits from Western Tianshan, Eastern Tianshan-Beishan and western Inner Mongolia.

Table 1 Geochronology of main epithermal and orogenic gold deposits in CAOB during Late Carboniferous-Early Permian.

District1	Name of deposit	Type	Dating method	Ages/Ma	Data sources
Altay	Duolanasayi	OGR	Ar-Ar (muscovite)	292.9±1.0	Xiao et al.,2003; Yan et al.,2004
			K-Ar(muscovite)	282.8±8.8	Xiao et al.,2003
			Re-Os(quartz inclusions)	269.0±13	Xiao et al.,2003
			Ar-Ar (muscovite)	293±4.8	Yan et al.,2004
			Ar-Ar (muscovite)	289	Li and Chen.,2004
	Saidu	OGR	Ar-Ar (muscovite)	278	Li and Chen.,2004
			Ar-Ar (muscovite)	291±8.4	Yan et al.,2004
			K-Ar(biotite)	297±3.3	Cheng et al.,1996
			K-Ar(muscovite)	294.7±3.5	Cheng et al.,1996
			Rb-Sr(quartz inclusions)	294±14	Li et al.,1998
			Rb-Sr(quartz inclusions)	305.6±7	Li et al.,1998
West Junggar	Hatu	EPI	Ar-Ar (quartz)	308.6±4.2	Shen et al.,1993
			Rb-Sr(quartz inclusions)	290±6.5	Li and Chen.,2004
			Rb-Sr(quartz inclusions)		Li and Chen.,2004
East Junggar	Shuangquan	OGR	Ar-Ar (sericite)	260±4	Xu et al.,2009
			Ar-Ar (sericite)	265±2	Xu et al.,2009
			Ar-Ar (sericite)	269±9	Xu et al.,2009
			Ar-Ar (sericite)	269±8	Xu et al.,2009
	Qingshui	OGR	-	C1	Lu et al.,2010; Xu et al.,2009
	Sarbulak	OGR	Rb-Sr	271±30	Li et al.,1998
			Pb-Pb	304±7	Li et al.,1998
	Kekesayi	OGR	Rb-Sr	227±24	Yin et al.,1998
	Kubusu	OGR	Rb-Sr	269±1	Li et al.,2004
	Yemaquan	OGR	Rb-Sr	300±46	Li et al.,2004
	Dongheishan	EPI	-	C1	Li et al.,2004
	Suoerbasitao	EPI	-	C1	Yang et al.,2009
	Jinshangou	OGR	-	C1	Peng et al.,2004;Lu et al.,2010

Western Tianshan	Sawayaerdun	OGR	Ar-Ar (quartz)	210.59±0.99	Wang.,2008;Zhang et al.,2012
			Ar-Ar (quartz)	209.07±0.71	Wang.,2008;Zhang et al.,2012
			Ar-Ar (quartz)	208.33±0.55	Wang.,2008;Zhang et al.,2012
			Ar-Ar (quartz)	213-206	Liu et al.,2007
			Rb-Sr (fluid inc.)	288±50	Liu et al.,2007
			Rb-Sr (quartz inclusion)	231±10	Liu et al.,2007
			Ar-Ar (quartz)	210.59±.0.99	Liu et al.,2007
			Rb-Sr (quartz)	246±16	Liu et al.,2007
	Saridala	OGR	Ar-Ar (quartz)	277	Liu et al.,2010
			Ar-Ar (plagicalse)	256.38	Yuan et al.,2017
	Katbasu	EPI	Ar-Ar(sericite)	268.56±1.8	Gao et al.,2015
			Re-Os (pyrite)	310.9±4.2	Zhang et al.,2015
	Muruntau	OGR	Re-Os (arsenopyrite)	287.5±1.7	Morelli et al.,2007
			Sm-Nd isochron(scheelite)	279±18	Kempe et al.,2001
			Rb-Sr granitic pluton	287.1±4.6	Kostitsyn Y.,1996
			Rb-Sr granitic diorite	286.2±1.8	Kostitsyn Y.,1996
	Zarmitan	OGR	Re-Os (pyrite)	286±2	Seltmann et al.,2011
			K-Ar	269±4.2	Bortnikov et al.,1996, Abzalov, 2007
			Ar-Ar (sericite)	245-220	
	Kumtor	OGR	Ar-Ar (sericite)	285	Mao et al.,2004
	Kumtor	OGR	Ar-Ar (ore include sericite)	288.4±0.6	Mao et al.,2004
			Ar-Ar (绢英岩)	285.5±1.2	Mao et al.,2004
			Ar-Ar (sericite)	284.3±3.0	Mao et al.,2004
			Ar-Ar (sericite)	285.4±0.2	Mao et al.,2004
	Bakyrchik	OGR	Ar-Ar	310-280	Naumov et al..,2012
	Sekisovskoye	OGR	Ar-Ar (sericite)	306±3.8	Naumov et al..,2012
	Suzdal	OGR	Ar-Ar (sericite)	281±3.3	Naumov et al..,2012
Eastern Tianshan	Wangfeng	OGR	Ar-Ar (sericite)	250.9±3.0	Yuan et al.,2017
			Ar-Ar (sericite)	255.8±3.0	Yuan et al.,2017
			Rb-Sr (quartz)	310	Li et al.,1998
			Ar-Ar (muscovite)	268.8±5.4	Shu et al.,1998
	Kanggur	OG	Ar-Ar (sericite)	252.5±1.	Shen et al.,2014

		R		7	
			Ar-Ar (sericite)	261.0±1.0	Shen et al.,2014
			Rb-Sr isochron(alterd andesite)	290±5	zhang et al.,2002
			Rb-Sr (quartz)	282±16	zhang et al.,2002
			U-Pb(zircon in tonalite)	275±7	zhang et al.,2002
			Sm-Nd isochron(magnetite-pyrite)	290.4±7.2	Zhang et al.,2004
			Rb-Sr isochron(quartz)	282.3±5	Zhang et al.,2004
			Rb-Sr isochron(quartz)	258±21	Zhang et al.,2004
			Rb-Sr isochron(quartz)	254±7	Zhang et al.,2004
			K-Ar(whole rock)	263.9±5	Chen et al.,2007
			K-Ar(whole rock)	261.4±4.4	Chen et al.,2007
			K-Ar(whole rock)	253.3±6.4	Chen et al.,2007
			Ar-Ar (sericite)	252.5±1.7	Chen et al.,2007
			Ar-Ar (sericite)	261.0±1.0	Chen et al.,2007
	Hongshi	OGR	Ar-Ar (sericite)	253.9±1.8	Chen et al.,2007
		OGR	Ar-Ar (sericite)	258.7±1.3	Chen et al.,2007
	Hongshan	OGR	Ar-Ar (sericite)	246.9±1.4	Chen et al.,2007
		OGR	Ar-Ar (sericite)	246.5±1.1	Chen et al.,2007
	Xifengshan	EPI	Rb-Sr isochron(fluid inclusion in quartz)	272±3	Zhang et al.2004
West Inner Mongolia	Xiaerchulu	EPI	Re–Os (molybdenite)	261±1.5	Wang et al.,2016
			U-Pb (zircon in grannitic)	271-269	Wang et al.,2016
			Re–Os (molybdenite)	263.8±4.4	Wang et al.,2014
	Zhulazhaga	EPI	Rb-Sr isochron (ore)	275±6	Wang et al.,2001
	Zhulazhaga	EPI	K-Ar (grannitic)	291.48±4.2	Wang et al.,2001
			U-Pb (zircon in grannitic)	280±6	Li.,2006
			U-Pb (zircon in grannitic)	279.7±5.2	Li.,2006
			Ar-Ar (quartz)	282.3 ± 0.9	Li et al., 2004
	Shalamiao	EPI	Re–Os (molybdenite)	266.8±3.9	Wang et al., 2007
	Hulunxibai	EPI	U-Pb (zircon in vein)	231.0±8.4	Li.,2006
			U-Pb (zircon)	219.5±8.8	Li et al., 2004
	Changshanhao	EPI	Ar-Ar (biotite)	256.3±1.8	Cao et al.,2014

			Ar-Ar (muscovite)	250.9±1.5	Cao et al.,2014
			Ar-Ar (muscovite)	246.0±1.6	Cao et al.,2014
			U-Pb (zircon)	290.9±2.8	Xiao et al.,2012
			U-Pb (zircon)	287.5±1.9	Xiao et al.,2012
			U-Pb (zircon)	277.0±3.0	Luo et al.,2009
			U-Pb (zircon)	267.9±1.2	Xiao et al.,2012
			Ar-Ar (biotite)	270.1±2.5	Wang et al.,2011
Beishan	Laodonggou	EPI	U-Pb (zircon)	243±1.0	Zhang et al.,2021
			U-Pb (zircon)	233.8±0.9	Zhang et al.,2021
			U-Pb (zircon)	237.8±1.2	Zhang et al.,2021
	Xiaoxigong	EPI	K-Ar(alkali feldspar granite)	306±4	Cui et al.1996
			K-Ar(orthophyre)	289±5	Cui et al.1996
			K-Ar(sericite)	276±7	Nie.,2003
			K-Ar(quartz)	284±4	Nie.,2003